Estimation of InSAR Tropospheric Delay Using ERA-Interim Global Atmospheric Reanalysis

O. Ku

***Abstract*—Tropospheric delays are considered to be one of the main performance limitations for Interferometric Synthetic Aperture Radar technology when applied to ground deformation monitoring. In this study, we evaluate the performance of ERA-Interim global atmospheric reanalysis on estimating the tropospheric delay on Sentinel-1 InSAR observations. The results are validated by four D-InSAR interferograms with small temporal/perpendicular baselines computed from Sentinel-1 observations. Based on the study, we concluded that the ERA-Interim global atmospheric reanalysis has relatively better performance in the regions with significant topography and stable atmospheric conditions.**

***Index Terms*—InSAR, tropospheric delay, water vapor mapping, atmosphere correction, ERA-Interim atmospheric reanalysis**

I. INTRODUCTION

IN the last twenty years, Interferometric Synthetic Aperture Radar (InSAR) technique has evolved into an important geodetic tool to measure movements and deformations of the Earths surface that are triggered by various geophysical phenomena, e.g. volcano activities (Lu et al., 2007; Hooper et al., 2007), permafrost change (Bell et al., 2008), ground water extraction (Kampes, 2006) and oil/gas production (Ketelaar, 2009).

Despite many successful case studies, the performance of InSAR is limited by the influence of electromagnetic path delay variations when the signal is propagating through the atmosphere (Hitney et al., 1985). Due to the layers of atmosphere, the atmospheric delay can be classified into two parts, the *ionospheric delay* and the *tropospheric delay*. In this study, we focus on the tropospheric delay part.

InSAR techniques measure the spatial and temporal variation of the SAR signal phase in order to extract ground surface deformation. The InSAR observations are the double differences w.r.t a reference point and a reference epoch. Due to the double-difference procedure, tropospheric artifacts in InSAR data are mainly caused by water vapor, which use the major spatio-temporally variable component of atmosphere, while other tropospheric delay components largely cancel out.

The delay caused by water vapor has been studied from many different aspects. For example, it can be measured from external sources, such as dense networks of GNSS stations (Li et al., 2006; Onn and Zebker, 2006) or space-borne multispectral scanners (Moisseev and Hanssen, 2003; Li et al., 2005, 2009). Alternative methods are using time series of SAR imagery to filter tropospheric artifacts based on the spatio-temporal statistics of tropospheric water vapor distributions (Ferretti et al., 2001; Berardino et al., 2002). Besides the above two methods, numerical weather prediction (NWP) models are widely regarded as a promising tool for estimating the tropospheric delays, as they can provide knowledge of the tropospheric conditions at the time of Synthetic Aperture Radar data acquisition. In this study, we focus on using one of the NWP models to estimate the tropospheric delay in InSAR observations.

In the past few years, NWP models have become an important potential data source for atmospheric correction of remote sensing data. Many studies have evaluated the application of NWPs for tropospheric delay correction on the InSAR measurements from ENVISAT ASAR (Foster et al., 2013; Gong et al., 2015), TerraSAR-X (Jehle et al., 2008), and RADARSAT-1 (Young and Sikora, 2010), and found that NWPs are often able to estimate the effects related to tropospheric stratification (Liu et al., 2009), and have less capability on estimating the effect of turbulence (Gong et al., 2015). However, less studies have been done on evaluating the performance of NWP models on wide-swath Sentinel-1 data. Under the Interferometric Wide Swath mode (IW mode), Sentinel-1 can acquire SAR images with a swath width of 250 km, which is significantly wider than the SAR acquisitions from other satellites. In this case, the tropospheric delay in SAR acquisitions may contain a large-scale variation in the spatial domain. This might be more easily captured by NWP models than small-scale variations. In this study, we will evaluate the performance of one of the NWP models, ERA-Interim global atmospheric reanalysis, on estimating and correcting the tropospheric delay in the InSAR results. ERA-Interim provides atmospheric physical parameters, which can be converted to tropospheric delay in InSAR acquisitions. Four Differential InSAR (D-InSAR) interferograms are computed to evaluate the performance of ERA-Interim, See Section II.

This study focuses on using the given ERA-Interim global atmospheric reanalysis to estimate the tropospheric delay in D-InSAR interferograms, produced by Sentinel-1 SAR images acquired under IW mode. It will not focus on the methodology of establishing a NWP model. Also this study will focus on the tropospheric delay. Moreover, the ionospheric effect will not be discussed in this paper. The study of tropospheric delay will be limited to the differential interferograms between two SAR images. The tropospheric effect on InSAR deformation time series will not be discussed.

A short description of the background of the two study sites, as well as the InSAR test data, and the ERA-Interim global atmospheric reanalysis will be introduced in Section II. The theory of estimating tropospheric delay from atmospheric physical parameters will be introduced in Section

O. Ku is with the Department of Geosciences and Remote Sensing, Delft University of Technology, 2628CD, Delft, the Netherlands.

III. In Section IV, we evaluate the performance of ERA-Interim global atmospheric reanalysis on estimating InSAR tropospheric delay, by comparing the estimated tropospheric delay to InSAR observations acquired from Sentinel-1 data. The conclusions and discussions are presented in Section V.

II. DESCRIPTION OF DATA AND STUDY AREAS

To evaluate the performance of ERA-Interim, we choose four test D-InSAR interferograms computed from Sentinel-1 SAR acquisitions on two test sites, and compute the tropospheric delay map based on ERA-Interim global atmospheric reanalysis. In this section we introduce the data used in this study, and the background of the two test sites.

A. Study Sites

In this study, we use the D-InSAR interferograms over two test sites as the test data to evaluate the performance of ERA-Interim. One test site is at the southern Netherlands area, the other one is at Wyoming state, USA. The location of the two test sites, and the coverage of interferograms in two test sites are shown in Figure 1. The Digital Elevation Models (DEM) of both test sites are shown in Figure 2.

1) The Netherlands: See the left figure of Figure 1. Most of the topography in this region is smooth. The average evolution of this region is 72 meters. The mountain areas are mainly distributed at the south-east region of this area. A rapid dynamic atmosphere condition, and more turbulent mixing effect than stratification effect is expected in this region (Hanssen, 2001).

2) Wyoming: See the right figure of Figure 1. Significant mountain topography exists in this area. The average evolution in this area is around 1510 meters. The atmospheric condition shows significant correlation with the topography in the area (Zhang, 1988).

B. D-InSAR data

Four differential interferograms computed from Sentinel-1 SAR acquisitions are used as reference to validate the quality of the ERA-Interim results. All the four interferograms have small temporal baselines (≤ 25 days) and small perpendicular baselines ($\leq$ 165 meters), therefore we assume no large-scale deformation signal exists in the interferograms. The topography component in each interferogram is removed based on the external 30 m resolution DEM from Shuttle Radar Topography Mission (SRTM). After removing the topographic phase. Under the assumption that the phase unwrapping is properly performed, the interferograms are expected to be dominantly representing the atmospheric delay signal, and used as a reference to evaluate the performance of ERA-Interim.

The information of the four interferograms is show in Table I. We give codes to each interferogram according to their location. The two interferograms in the Netherlands are coded as NL1, and NL2, while the two interferograms in Wyoming, USA are coded as WY1 and WY2.

TABLE I: the list of four interferograms used in this study

Code	Master date (yyyy-mm-dd)	Slave date (yyyy-mm-dd)	UTC Time	Perpen--dicular baseline (m)	Temporal baseline (day)
NL1	2015-07-14	2015-07-26	17:24	23	12
NL2	2015-10-18	2015-10-30	17:24	120	12
WY1	2015-07-05	2015-07-29	13:16	165	24
WY2	2015-10-09	2015-11-02	13:16	40	24

C. ERA-Interim Global Atmospheric Reanalysis

ERA-Interim is a global atmospheric reanalysis produced by the European Centre for Medium-Range Weather Forecasts (ECMWF). It provides atmospheric reanalysis data from 1979, continuously updated in real time. It is public available at http://apps.ecmwf.int/datasets/. The system produces a 4-D atmospheric dynamic analysis with a 12-hour analysis window, and with a horizontal resolution of approximately 80×80 km. In vertical direction, it has 37 pressure levels with a resolution of 5 hPa (Jolivet et al., 2014).

The Sentinel-1 SAR image IW mode has a resolution of approximately 20×5 meters. The resolution of ERA-Interim is significantly lower than the resolution of Sentinel-1 SAR image. This low resolution means that the ERA-Interim may not be able capture the small scale turbulent mixing effect in InSAR observations. However, since the DEM used in this study have a resolution of 30×30m, this means ERA-Interim may have good capability to estimate stratification effect, which is significantly related to the topography (Hanssen, 2001). In this study, the performance of ERA-Interim will be evaluated for both turbulence-dominant case and stratification-dominant case.

ERA-Interim provides various physical parameters of atmospheric dynamics. Below are the parameters extracted from ERA-Interim to estimate the tropospheric delay:

- Partial pressure of dry air P_d, in hPa;
- Partial pressure of water vapor e, in hPa;
- Atmospheric temperature T, in Kelvin (K);
- Density of liquid water content W, in g/m^3.

Table II lists the dates of ERA-Interim global atmospheric reanalysis data used in this study. The date of the ERA-Interim data is chosen according to the acquisition date of the Sentinel-1 SAR images.

ERA-Interim provides the atmospheric physical parameters at UTC time 0:00, 6:00, 12:00 and 18:00 every day, with an analysis window of 12 hours. Within the time period of each analysis window, the atmospheric reanalysis is performed to derive the atmospheric parameters, based on multi-source observations acquired in this period. To acquire the atmospheric physical parameters at the SAR acquisition time, we assume the atmospheric parameters change linearly between two adjacent epoch of ERA-Interim, and linearly interpolate the value at SAR acquisition time based on ERA-Interim data at adjacent epochs, as shown in Table II.

III. ESTIMATION OF TROPOSPHERIC DELAY

In this Section, we introduce the theory of converting atmospheric physical parameters provided by ERA-Interim

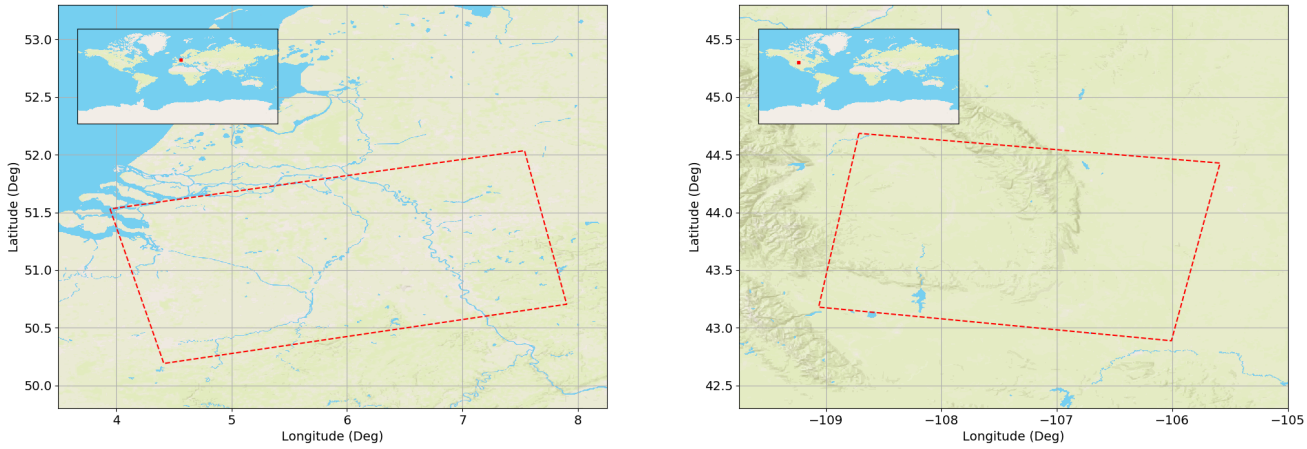

Fig. 1: An overview of the two test sites. Left figure: the test site in the Netherlands. Right figure: the test site in Wyoming, USA. The red dot in the upper left world map of each figure indicates the approximate location of each test site. The red polygon dashed shows the coverage of the interferogram in each test site.

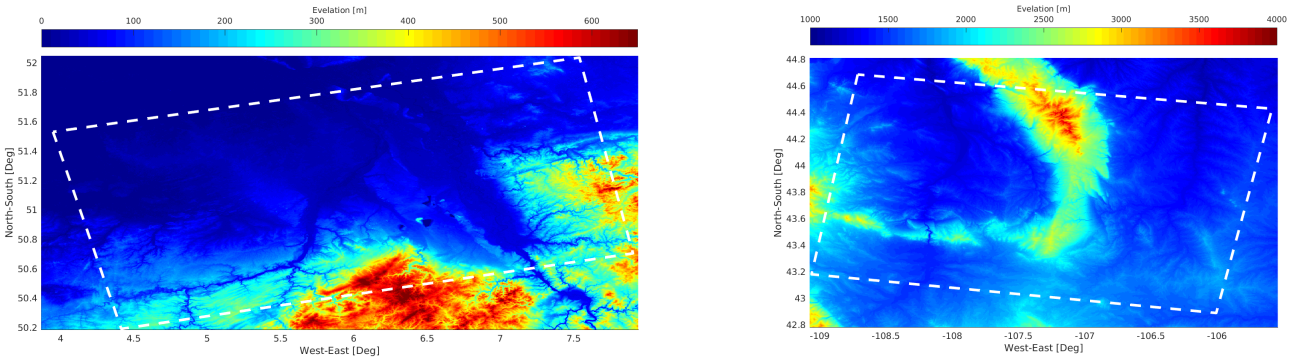

Fig. 2: Left: the DEM of the Netherlands study sites. Right: the DEM of the Wyoming study sites. The DEM data is acquired by Shuttle Radar Topography Mission (SRTM). In both test sites the DEM data have the resolution of 30×30 m, and is under WGS84 coordinate system. he white polygon dashed shows the coverage of the interferogram in each test site.

TABLE II: the date list of era-interim data

Date (year-month-day)	UTC time (hours:minute)	Corresponding SAR acquisition
2015-07-05	12:00	WY1, master
2015-07-05	18:00	WY1, master
2015-07-14	12:00	NL1, master
2015-07-14	18:00	NL1, master
2015-07-26	12:00	NL1, slave
2015-07-26	18:00	NL1, slave
2015-07-29	12:00	WY1, slave
2015-07-29	18:00	WY1, slave
2015-10-09	12:00	WY2, master
2015-10-09	18:00	WY2, master
2015-10-18	12:00	NL2, master
2015-10-18	18:00	NL2, master
2015-10-30	12:00	NL2, slave
2015-10-30	18:00	NL2, slave
2015-11-02	12:00	WY2, slave
2015-11-02	18:00	WY2, slave

global atmospheric reanalysis into tropospheric delay.

The tropospheric delay experienced by a microwave signal can be caused by two terms: 1) the velocity variations along the signal's line-of-sight (LOS) direction between antenna and scatter, and 2) the induced bending of the signal propagation path (Bean and Dutton, 1968). When the incidence angle of signal is less than 87°, the bending effect can be ignored (Bean and Dutton, 1968), and the LOS tropospheric delay can be considered into a function of only the variation of propagation velocity. This velocity variation is closely related to the vertically integrated troposphere refractivity variations, and can be written as (Hanssen, 1998)

$$S_k^{t_i} = 10^{-6} \int_{H_0}^{H} \frac{N_{k,t_i}^h}{\cos\theta_{inc}^k} \, \mathrm{d}h, \tag{1}$$

where $S_k^{t_i}$ in mm is the LOS tropospheric delay for the resolution cell k at the acquisition time t_i, θ_{inc}^k in degree is the incidence angle of the radar signal for the resolution cell k, H_0 is the ground elevation, and H in km is the elevation of the upper boundary of the troposphere layer. In this study, we use the experience value 15 km for H (Saastamoinen, 1972). The refractivity N_{k,t_i}^h can be written as (Smith and Weintraub, 1953; Kursinski et al., 1997)

$$N_{k,t_i}^h = k_1 \frac{P_{k,t_i}^h}{T_{k,t_i}^h} + k_2 \frac{e_{k,t_i}^h}{T_{k,t_i}^h} + k_3 \frac{e_{k,t_i}^h}{(T_{k,t_i}^h)^2} + k_4 W_{k,t_i}^h, \tag{2}$$

where the dimensionless term N^h_{k,t_i} is the refractivity for resolution cell k at acquisition time t_i, on the elevation of h. T^h_{k,t_i} in Kelvin is the atmospheric temperature. Two pressures P^h_{k,t_i} and e^h_{k,t_i} in hPa are respectively the total atmospheric pressure and the partial water vapor. W^h_{k,t_i} in g/m^3 is the density of water vapor content. P^h_{k,t_i}, e^h_{k,t_i} and W^h_{k,t_i} are for resolution cell k at acquisition time t_i, on the elevation of h. Four constants values $k_1 = 77.6$ K/hPa, $k_2 = 23.3$ K/hPa, $k_3 = 3.75 \times 10^5$ K^2/hPa and $k_4 = 1.4$ m^3/g.

As introduced in Section II, ERA-Interim global atmospheric reanalysis provides a 4-D reanalysis of various atmospheric dynamic parameters, i.e. P^h_{k,t_i}, e^h_{k,t_i} and W^h_{k,t_i} are known. Based on Eq. (1) and Eq. 2, for each k the tropospheric delay can be computed. For a interferogram between acquisitions at two epochs t_i and t_j, the effect of tropospheric delay for resolution k can be written as

$$\triangle S_k^{t_i,t_j} = S_k^{t_i} - S_k^{t_i}, \tag{3}$$

where $S_k^{t_i,t_j}$ is the effect of tropospheric delay of interferogram between acquisitions at t_i and t_j for resolution cell k, estimated from ERA-Interim global atmospheric reanalysis.

IV. Results and Discussion

We evaluate the performance of ERA-Interim global atmospheric reanalysis on estimating the tropospheric delay, by comparing the ERA-Interim estimation with D-InSAR interferograms.

A. Experiment results

The atmospheric parameters, i.e. T^h_{k,t_i}, P^h_{k,t_i}, e^h_{k,t_i} and W^h_{k,t_i} can be provided with a horizontal resolution of 80 km, a vertical equi-pressure resolution of 5 hPa, and a temporal resolution of 6h. The ground elevation H_0 in Eq. (1) is given by the external SRTM with a resolution of 30×30 m. We use the resolution cell of DEM data as k in Eqs. (1) and (2). To compare the tropospheric delay estimation from ERA-Interim with the D-InSAR results, we take the following three steps to convert them into the same spatio-temporal reference system:

1) ***Temporal interpolation of ERA-Interim data***. ERA-Interim has an analysis window of 6 hours. To acquire the atmospheric parameters at the time of SAR acquisition, we linearly interpolate the atmospheric parameters at Sentinel satellite passing time, based on ERA-Interim data before (at 12:00) and after (at 18:00) the SAR acquisitions. For instance, for a certain atmospheric parameter x at SAR aquisition time t_{SAR}, its value can be estimated by

$$x_{\text{SAR}} = x_{t_1}\frac{t_{\text{SAR}} - t_1}{t_2 - t_1} + x_{t_2}\frac{t_2 - t_{\text{SAR}}}{t_2 - t_1}, \tag{4}$$

where $x_{t_{\text{SAR}}}$ is the value of x on SAR acquisition time. t_1 and t_2 are respectively the two epochs before and after t_{SAR}, on which ERA-Interim provides data. x_{t_1} and x_{t_1} are the values of x on t_1 and t_2 respectively.

2) ***Spatial interpolation of ERA-Interim data.*** ERA-Interim provides 60 vertical layers of atmospheric physical parameters, with approximately 80 km horizontal resolution. On each vertical layer, we use 2-D bi-linear interpolation to interpolate the ERA-Interim data into the same grid system of SRTM DEM.
3) ***Down-sampling of D-InSAR data.*** The D-InSAR interferogram is computed based on Sentinel-1 SAR acquisitions, with a resolution of approximately 25×25 meters. To compare the D-InSAR interferograms with ERA-Interim results, we down sample the D-InSAR interferograms to the same grid system of SRTM DEM, using a bi-linear interpolation method.

After converting the ERA-Interim and D-InSAR results into the same spatio-temporal reference system, we estimate the tropospheric delay based on Eqs. (1) to (3) for the four pre-selected Sentinel-1 interferograms, and compare the estimation with D-InSAR results. The tropospheric delay estimation and the D-InSAR results are shown in Figure III.

In Table III, four interferograms and the corresponding tropospheric delay map are shown. In the Wyoming study case, interferogram WY1 and WY2 show significant similarity with ERA-Interim estimation. The correlation between the estimated tropospheric delay map and the D-InSAR results are computed. For WY1 this correlation is 0.78, and for WY2 the correlation is 0.66. On the other hand, in the Netherlands study case, interferogram NL1, and NL2 do not show clear similarity with the ERA-Interim estimation of tropospheric delay. The correlation of NL1 and NL2 with their corresponding tropospheric map, is respectively 0.12 and 0.09.

It should be noted that due to the low spatial resolution (80 km) of ERA-Interim data, the tropospheric delay estimation is mainly contributed by DEM, which has the resolution of 30 m. Therefore in the Wyoming study site, which has the significant topography variation, the two estimations of tropospheric delay show significant small scale, local changes. While in the Netherlands case, especially at the coastal area, due to the smooth topography, less small scale variation shows in the the tropospheric delay map.

Figure 3 shows the interferograms after correcting tropospheric delay using the estimation of ERA-Interim.

In Figure 3, after correcting tropospheric delay using the estimation from ERA-Interim data, the residuals in NL1 and NL2 still have significant large scale variation, while in WY1 and WY2, the residuals mainly show small scale patterns, and the overall magnitude of which is much smaller. We compute the root mean square (RMS) values for the four corrected interferograms. The RMS values are 3.27 mm, 4.24 mm, 0.68 mm and 1.52 mm respectively for NL1, NL2, WY1 and WY2 respectively. The RMS values for Wyoming case are smaller than the Netherlands case.

B. Discussion

As shown in Table I, all the four interferograms in this study, i.e. NL1, NL2, WY1 and WY2, have small temporal baselines and spatial baselines. Therefore, we assume that after subtracting topography component and correcting orbit trend, and under the assumption that the interferogram is properly unwrapped, the interferogram will mainly contain the tropospheric delay signal.

Code	ERA-Interim estimated tropospheric delay	D-InSAR interferogram
NL1	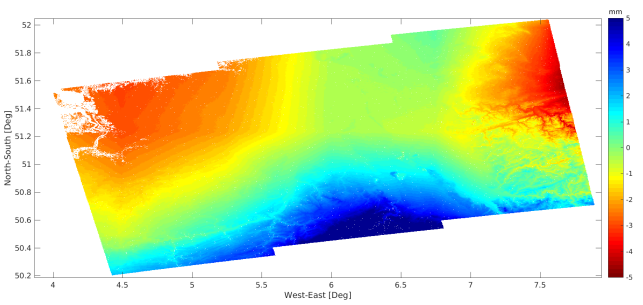	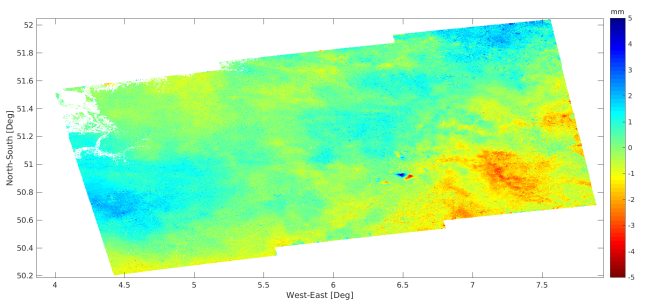
NL2	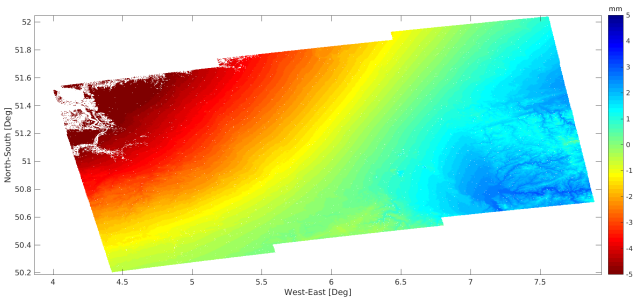	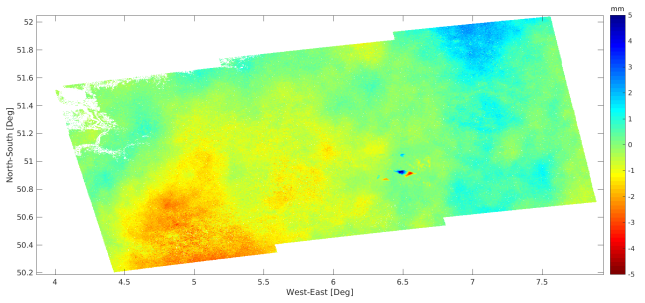
WY1	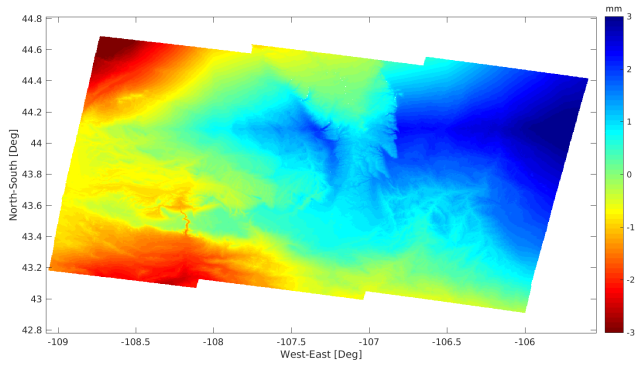	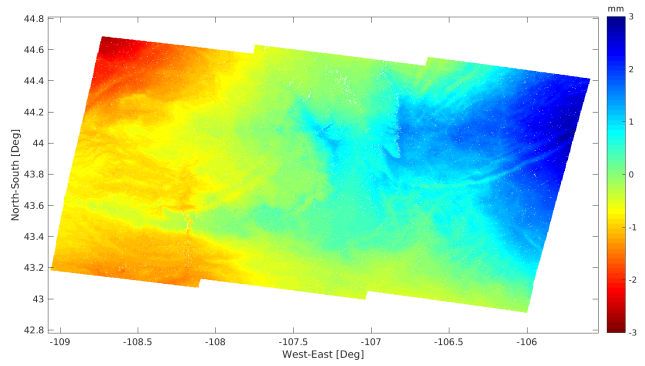
WY2	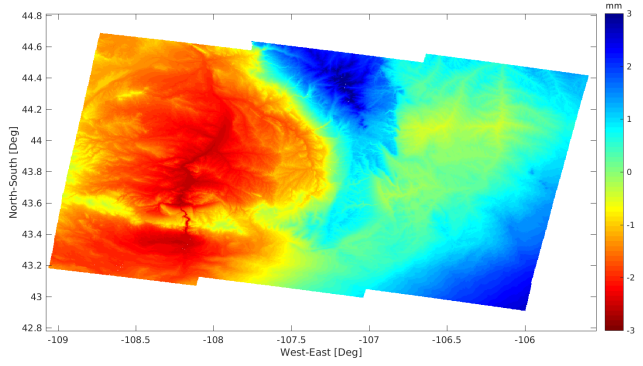	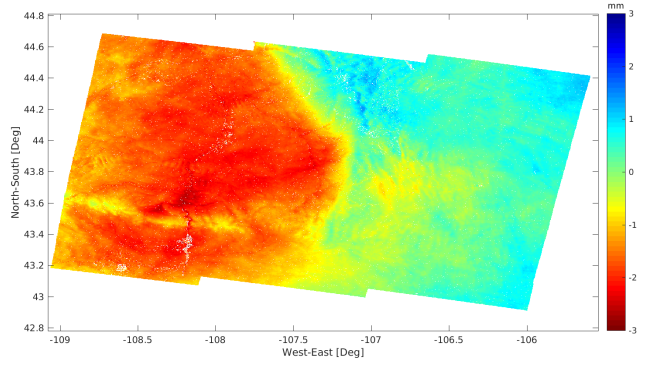

TABLE III: Four D-InSAR interferograms computed from Sentinel-1 SAR data, and the corresponding tropospheric delay map estimated from ERA-Interim atmospheric reanalysis. The NL1 and NL2 are the two study cases in the Netherlands. The WY1 and WY2 are the two study cases in Wyoming, USA. Both ERA-Interim and the D-InSAR interferograms are in the WGS-84 coordinate system, and resampled into the same grid system. The unit of the tropospheric delay is mm.

The WY1 and WY2 D-InSAR results show good correlation with the tropospheric delay map estimated from ERA-Interim data. Both the tropospheric delay map and D-InSAR results show a good correlation with topography, two reasons are likely to cause the spatial distribution of the tropospheric delay in these two interferograms: 1) the stratification effect dominants the atmospheric delay, which mainly changes on the vertical direction but not horizontal direction, and is strongly correlated with topography. 2) the atmospheric delay is affected by the orographic shielding effect, i.e. the mountains in the area block the component in the atmosphere which causes delay to the west side of the mountain.

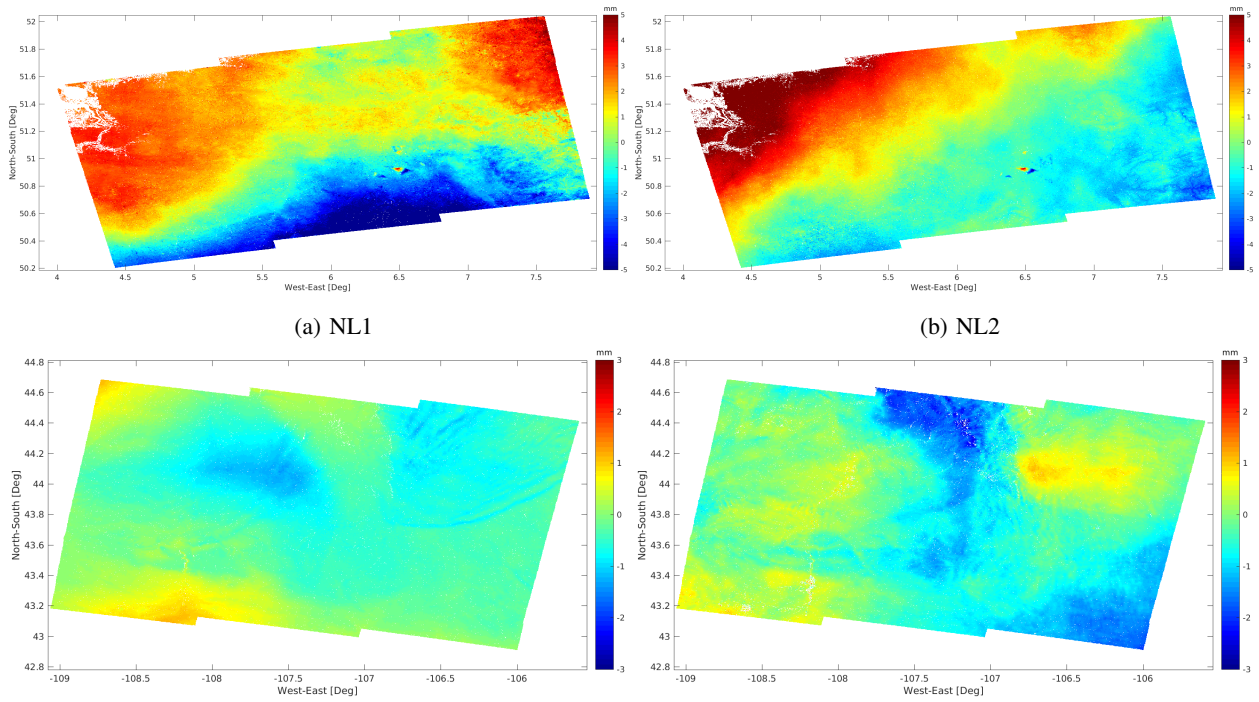

(a) NL1 (b) NL2

(c) WY1 (d) WY2

Fig. 3: D-InSAR interferograms after correcting the tropospheric delay. The correction is performed by subtracting the tropospheric delay map from the D-InSAR results. The tropospheric delay map is estimated using ERA-Interim atmospheric reanalysis data. The RMS values are 3.27 mm, 4.24 mm, 0.68 mm and 1.52 mm for NL1, NL2, WY1 and WY2, respectively.

After correcting the tropospheric delay, there is less residual signal left in WY1, ans all the residuals show in small patterns in spatial domain, which can be the remaining tropospheric delay signal caused by turbulence effect. In WY2, there are relatively large residuals in the mountain region, which could be caused by the over-correction of tropospheric delay estimation. After correcting tropospheric delay, we do not find significant trends in WY1 and WY2.

The NL1 and NL2 D-InSAR results, on the other hand, do not show correlation with tropospheric delay map. The following four factors may limit the performance of tropospheric delay estimation in this study sites:

- ***Rapid dynamics of the atmosphere condition in temporal domain.*** The ERA-Interim provides atmospheric parameters at every 6 hours. To acquire the atmospheric parameters at the SAR acquisition time, we use the linear interpolation method. This method intrinsically assumes that the atmosphere condition changes linearly between two epochs of ERA-Interim. When the atmospheric condition changes rapidly in time, the atmospheric parameters can not be effectively estimated at the SAR acquisition time. Therefore the performance of ERA-Interim may not be satisfying due to the insufficient temporal resolution.
- ***Low spatial resolution of ERA-Interim data.*** The ERA-Interim atmospheric reanalysis has a resolution of 80 km. According to previous studies (Hanssen, 2001; Treuhaft and Lanyi, 1987), the spatial variation regimes of tropospheric delay can have a scale from 0.01 km to as large as 3000 km. The resolution of DEM, which is 30×30 m, can aid on estimating the tropospheric delay dependent on topography. However, if the tropospheric delay has smaller signal and not correlated with topography, the estimation based on ERA-Interim data will be poor.
- ***The flaws in the reanalysis of ERA-Interim model.*** ERA-Interim model perform the reanalysis of atmospheric parameters in an 12-hour analysis window, based on the related observations from multiple measurements e.g. sounding balloons, ground-based Doppler radar, etc. The errors in the measurements and the imperfection of the physical model may cause the errors in the atmospheric parameters provided by ERA-Interim, and therefore results into the limited performance on estimating tropospheric delay.
- ***Effect of correcting orbit error.*** The NL1 and NL2 interferogram show significant differences with the ERA-Interim estimation. This differences may also result from correcting orbit error when processing Sentinel-1 data. When removing the orbit error, we estimated a 2-D linear signal in horizontal direction (an estimated ”plane”), and remove this signal from interferogram. This may results into removing the large scale atmospheric signal which linear distributed in space.

In Figure 3, after correcting tropospheric delay, there are clear trends existing in both interferograms. It is likely that the application of ERA-Interim estimation in this case introduce even more errors in the InSAR observations.

V. Conclusion and Recommendation

In this study, we evaluated the performance of ERA-Interim data on correcting tropospheric delay in D-InSAR interferograms,by comparing the estimated tropospheric delay map with D-InSAR results.

The D-InSAR results over the Wyoming test sites show good correlation with the estimated tropospheric delay map. Based on the correlation ratio and D-InSAR results after correcting atmospheric phase, we conclude that the ERA-Interim atmospheric reanalysis has a good performance on estimating tropospheric delay in this region. Considering the atmospheric condition in this area (Zhang, 1988), the good performance can be resulted from the dominant stratification effect, or the orographic effect of this region.

The D-InSAR results over the Netherlands test sites, on the other hand, do not show significant correlation with the estimated tropospheric delay map. Four possible causation are given in Section IV-B, i.e. the rapid change of atmospheric condition, the Low spatial resolution of ERA-Interim data, The flaws in the reanalysis of ERA-Interim model, and the effect of correcting orbit error.

Based on the study of four interferograms over two test sites, we evaluated the performance of ERA-Interim atmospheric reanalysis on estimating tropospheric delay. The conclusion is that the ERA-Interim atmospheric reanalysis has good performance on correcting the tropospheric delay in Sentinel-1 D-InSAR results, when the tropospheric delay show good correlation with topography.

However, in case of small scale tropospheric delay, or the atmospheric condition changes rapidly, the performance of ERA-Interim atmospheric is limited.

Several potential improvements remains for the future study on this topic:

- ***Taking into account the influence of ionospheric delay.*** The ionospheric and the tropospheric delay effect together make up the atmospheric delay in InSAR observations (Hanssen, 2001). In this study, we assume the tropospheric delay signal is the main component in D-InSAR results, the influence of the ionospheric signal is ignored.
- ***Evaluate the performance of ERA-Interim on more study cases.*** In this study, we use four Sentinel-1 interferograms as study case, which is a limited number. More case studies should be applied for a solid evaluation of ERA-Interim's performance on correcting tropospheric delay on Sentinel-1 interferograms.

References

Bean, B. R. and Dutton, E. J. (1968). *Radio Meteorology*. Dover, New York.

Bell, J. W., Amelung, F., Ferretti, A., Bianchi, M., and Novali, F. (2008). Permanent scatterer insar reveals seasonal and long-term aquifer-system response to groundwater pumping and artificial recharge. *Water Resources Research*, 44(2).

Berardino, P., Fornaro, G., Lanari, R., and Sansosti, E. (2002). A new algorithm for surface deformation monitoring based on small baseline differential SAR interferograms. *IEEE Transactions on Geoscience and Remote Sensing*, 40(11):2375–2383.

Ferretti, A., Prati, C., and Rocca, F. (2001). Permanent scatterers in SAR interferometry. *IEEE Transactions on Geoscience and Remote Sensing*, 39(1):8–20.

Foster, J., Kealy, J., Cherubini, T., Businger, S., Lu, Z., and Murphy, M. (2013). The utility of atmospheric analyses for the mitigation of artifacts in insar. *Journal of Geophysical Research: Solid Earth*, 118(2):748–758.

Gong, W., Meyer, F., Lee, C.-W., Lu, Z., and Freymueller, J. (2015). Measurement and interpretation of subtle deformation signals at unimak island from 2003 to 2010 using weather model-assisted time series insar. *Journal of Geophysical Research: Solid Earth*, 120(2):1175–1194.

Hanssen, R. (1998). *Atmospheric heterogeneities in ERS tandem SAR interferometry*. Delft University Press, Delft, the Netherlands.

Hanssen, R. F. (2001). *Radar Interferometry: Data Interpretation and Error Analysis*. Kluwer Academic Publishers, Dordrecht.

Hitney, H. V., Richter, J. H., Pappert, R. A., Anderson, K. D., and Baumgartner, G. B. (1985). Tropospheric radio propagation assessment. *Proceedings of the IEEE*, 73(2):265–283.

Hooper, A., Segall, P., and Zebker, H. (2007). Persistent scatterer interferometric synthetic aperture radar for crustal deformation analysis, with application to Volcán Alcedo, Galápagos. *Journal of Geophysical Research*, 112(B7):B07407.

Jehle, M., Perler, D., Small, D., Schubert, A., and Meier, E. (2008). Estimation of atmospheric path delays in terrasar-x data using models vs. measurements. *Sensors*, 8(12):8479–8491.

Jolivet, R., Agram, P. S., Lin, N. Y., Simons, M., Doin, M.-P., Peltzer, G., and Li, Z. (2014). Improving insar geodesy using global atmospheric models. *Journal of Geophysical Research: Solid Earth*, 119(3):2324–2341.

Kampes, B. M. (2006). *Radar interferometry*. Springer.

Ketelaar, V. B. H. (2009). *Satellite radar interferometry: Subsidence monitoring techniques*, volume 14. Springer Science & Business Media.

Kursinski, E. R., Haij, G. A., Schofield, J. T., and Linfield, R. P. (1997). Observing earth's atmosphere with radio occultation measurements using the global positioning system. *Journal of Geophysical Research*, 102(D19):23,429–23,465.

Li, Z., Fielding, E., Cross, P., and Preusker, R. (2009). Advanced insar atmospheric correction: Meris/modis combination and stacked water vapour models. *International Journal of Remote Sensing*, 30(13):3343–3363.

Li, Z., Fielding, E. J., Cross, P., and Muller, J.-P. (2006). Interferometric synthetic aperture radar atmospheric correction: Gps topography-dependent turbulence model. *Journal of Geophysical Research: Solid Earth*, 111(B2).

Li, Z., Muller, J.-P., Cross, P., and Fielding, E. J. (2005). Interferometric synthetic aperture radar (insar) atmospheric correction: Gps, moderate resolution imaging spectroradiometer (modis), and insar integration. *Journal of Geophysical Research: Solid Earth (1978–2012)*, 110(B3).

Liu, S., Mika, A., and Hanssen, R. (2009). On the value of

high-resolution weather models for atmospheric mitigation in SAR interferometry. In *International Geoscience and Remote Sensing Symposium, Town, South Africa, 12–17 July 2009*, page 4 pp.

Lu, Z., Dzurisin, D., Wicks, C., Power, J., Kwoun, O., and Rykhus, R. (2007). Diverse deformation patterns of aleutian volcanoes from satellite interferometric synthetic aperture radar (insar). *Volcanism and subduction: the Kamchatka region*, pages 249–261.

Moisseev, D. and Hanssen, R. (2003). Towards and atmosphere-free interferogram; first comparison between ENVISAT's ASAR and MERIS water vapor observations. In *International Geoscience and Remote Sensing Symposium, Toulouse, France, 21–25 July 2003*, pages cdrom, 4 pages.

Onn, F. and Zebker, H. (2006). Correction for interferometric synthetic aperture radar atmospheric phase artifacts using time series of zenith wet delay observations from a gps network. *Journal of Geophysical Research: Solid Earth*, 111(B9).

Saastamoinen, J. (1972). Introduction to practical computation of astronomical refraction. *Bulletin Geodesique*, 106:383–397.

Smith, Jr., E. K. and Weintraub, S. (1953). The constants in the equation for atmospheric refractive index at radio frequencies. *Proceedings of the I.R.E.*, 41:1035–1037.

Treuhaft, R. N. and Lanyi, G. E. (1987). The effect of the dynamic wet troposphere on radio interferometric measurements. *Radio Science*, 22(2):251–265.

Young, G. S. and Sikora, T. (2010). A sar-based nwp error warning product. In *17th Conference on Satellite Meteorology and Oceanography*.

Zhang, S. F. (1988). a critical evaluation of the von karman constant from a new atmospheric surface layer experiment.